journal

J. Am. Ceram. Soc., 79 [2] 313–20 (1996)

Effect of Loading Rate on the Monotonic Tensile Behavior of a Continuous-Fiber-Reinforced Glass-Ceramic Matrix Composite

Bent F. Sørensen

Materials Department, Risø National Laboratory, DK-4000 Roskilde, Denmark, European Union

John W. Holmes*

Ceramic Composites Research Laboratory, Department of Mechanical Engineering and Applied Mechanics, The University of Michigan, Ann Arbor, Michigan 48109-2125

The stress–strain behavior of a continuous-fiber-reinforced ceramic matrix composite has been measured over a wide range of loading rates (0.01 to 500 MPa/s). It was found that the loading rate has a strong effect on almost every feature of the stress–strain curve: The proportionality stress, the composite strength and failure strain increase with increasing loading rate. The microstructural damage varies also with the loading rate; with increasing loading rate, the average matrix crack spacing increases and the average fiber pullout length decreases. Using simple models, it is suggested that these phenomena are caused partly by time-dependent matrix cracking (due to stress corrosion) and partly by an increasing interfacial shear stress with loading rate.

I. Introduction

It is well-known that glasses and glass-ceramics are prone to time-dependent crack growth due to stress corrosion.[1] Time-dependent cracking behavior has also been observed in continuous-fiber-reinforced glass-ceramic matrix composites (CMCs).[2–4] The most detailed study on time-dependent matrix cracking in damage-tolerant CMCs is probably that by Spearing *et al.*[5] In their study, the matrix crack spacing was measured as a function of time (typically up to 10^5 s) in Nicalon SiC fiber-reinforced calcium aluminosilicate specimens subjected to a constant load (bending or tension). Although only one specimen was used per load level (as discussed further elsewhere,[6] there is, under identical loading conditions, a variation in matrix crack density from specimen to specimen), it was shown that the average crack spacing approached a saturated value between 0.08 and 0.13 mm for load levels in the range of 150 to 250 MPa. A similar saturated matrix crack spacing was also found for the same material system in static loading experiments performed by Sørensen and Holmes.[6]

Another parameter that may be sensitive to loading rate is the interfacial shear stress. In fiber pullout experiments, Goettler and Faber[7] measured the interfacial shear stress of SCS-6 SiC-fiber-reinforced soda borosilicate glass for various loading rates. The interfacial shear stress was found to increase with increasing loading rate. Lankford *et al.*[8] studied the stress–strain behavior of Nicalon SiC-fiber-reinforced lithium aluminosilicate (LAS) under very high loadings rates (impact) using a split Hopkinson pressure bar. Under very rapid loading rates the interfacial shear stress decreased, apparently due to melting of the matrix in the vicinity of the interface. In general, the frictional stress depends strongly on the wear mechanism. In steel, for instance, the friction coefficient is found to *decrease* with increasing loading rate.[9]

The purpose of our study was to perform a systematic investigation of the effect of loading rate on the room-temperature monotonic stress–strain behavior of damage-tolerant ceramic matrix composites.

II. Experimental Procedure

Nicalon SiC-fiber-reinforced calcium aluminosilicate glass-ceramic matrix composites (Corning Inc., Corning, NY, denoted Nicalon SiC_f/CAS II) were used in this study. The composites were produced with eight unidirectional plies. Edge-loaded tensile specimens (Fig. 1) were machined from flat plates using diamond tooling, such that the loading direction was parallel with the fiber direction. The specimen design and grip arrangement are described in detail elsewhere.[10] In order to allow observation of matrix cracking, each specimen was polished at a minor face parallel with the fiber direction. The polishing was performed by hand, using a 38 mm mandrel rotating at 1500 rpm. The following polishing procedure was used: (1) 600-grit SiC paper for 5 min; (2) 45-μm diamond paste for 5 min (nylon cloth), (3) 6-μm diamond paste for 5 min (nylon cloth), (4) 1.0-μm diamond paste for 10 min (nylon cloth).

The room-temperature (20°C, humidity 40% to 45%) stress–strain behavior was measured in uniaxial tension along the fiber direction for various loading rates, ranging from 0.01 to 500 MPa/s (corresponding to a strain rate of approximately 10^{-7} to 10^{-2} or a time-to-failure of approximately 10 h down to 1 s). Specimens were loaded using a servo-hydraulic test machine (Model 810, MTS Systems, Minneapolis, MN). The strain was measured by an MTS 632.11C-20 extensometer, which was modified for a 36 mm gauge length.

After the tensile tests, the matrix crack spacing of each specimen was measured at the polished face by optical microscopy along lines in the axial direction of the specimens. In order to enhance the visibility of matrix cracks, the light source was aimed parallel to the fibers. In order to obtain good reproducibility, at least 350 cracks were counted, since some variation was found in the extent of cracking from matrix domains to fiber-rich regions.

The fracture surfaces were inspected in an ElectroScan E-3 environmental scanning microscope (ESEM), and fiber pullout lengths were measured from micrographs taken with a 45° tilt angle. Between 300 and 600 fibers were measured per specimen along lines traversing the specimen from one major face to the other. A significant variation in fiber pullout length was observed over the fracture surface. Often the fiber pullout

F. W. Zok—contributing editor

Manuscript No. 192705. Received April 10, 1995; approved August 21, 1995.

Supported by the Engineering Science Centre at Risø for Structural Characterization and Modelling of Materials and the Air Force Office for Scientific Research. A portion of this study was performed when B.F.S. was a visiting research investigator at the University of Michigan.

*Member, American Ceramic Society.

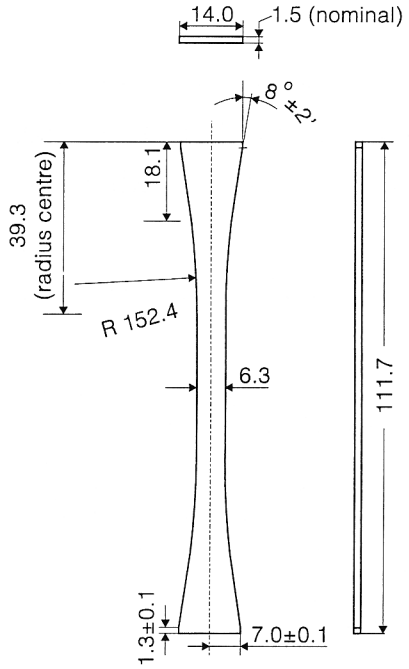

Fig. 1. Geometry of the edge-loaded tensile test specimens used in this study. All dimensions are in millimeters.

lengths were longest within a thin layer near the specimen faces. This edge effect was considered to be an artifact, perhaps resulting from the fact that most of these fibers were only partially embedded in the matrix. In order to minimize erroneous measurements, the fiber pullout lengths were measured along lines where such free surface effects were absent. A series of overlapping micrographs were taken, such that the fiber pullout length could be measured over a larger area.

III. Results

The monotonic stress–strain behavior for the various loading rates is shown in Fig. 2. All data plotted in this figure were obtained from specimens failed within the gauge section. Only one tensile curve is shown for each loading condition. Results from additional specimens that failed outside the gauge section were discarded. It was noted, however, that these stress–strain curves followed those shown in Fig. 2 very closely, although the failure stress and strain differed slightly. From Fig. 2 it can be seen that the stress–strain behavior is strongly dependent on the loading rate, influencing both the shape of the nonlinear stress–strain curve and the failure strain and strength.

Generally, the stress–strain response of unidirectional continuous fiber-reinforced CMCs can be divided into characteristic stages, reflecting the underlying damage mechanisms.[3] Stage I corresponds to fully linearly elastic behavior (low applied stress). Stage II denotes the formation of multiple matrix cracking, which leads to nonlinearity in the overall stress–strain curve. At higher stress level, the stress–strain curve enters its second linear part (Stage III), indicating that matrix cracking has reached a saturated level and that interfacial sliding takes place. Finally, distributed fiber failures may occur (Stage IV) before localization and specimen fracture. The Nicalon SiC_f/CAS II composite follows this characteristic behavior.[3]

Following Prewo,[11] the onset of nonlinearity within Stage II is quantified by the stress level $\sigma_{0.02}$ corresponding to a deviation of 0.02% in the strain from linear elasticity. We prefer to use $\sigma_{0.02}$ as a measure of nonlinearity instead of the first detectable nonlinearity on the stress–strain curve, since the latter depends strongly on the resolution of the load and strain transducers, whereas the former is much better defined. Neither of these stress values coincides with matrix crack initiation:

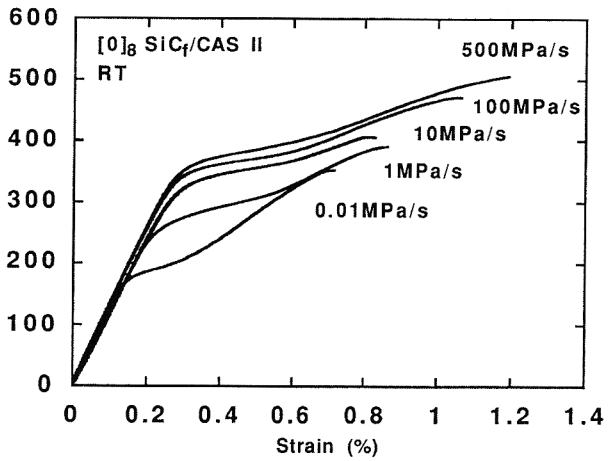

Fig. 2. Stress–strain behavior of unidirectional Nicalon SiC_f/CAS II for various loading rates. Note that an increasing loading rate increases the proportional limit, the strength and failure strain, and toughness.

Detailed experimental studies on matrix crack initiation[3,12] by acoustic emission and replica techniques have shown that the first matrix cracking occurs *without* a detectable compliance change. A similar conclusion has also been reached by accurate modeling of the matrix cracking process.[13] Figure 3(a) shows $\sigma_{0.02}$ as a function of the loading rate. Clearly, an increasing loading rate leads to a higher value for $\sigma_{0.02}$.

The average matrix crack spacing is shown in Fig. 3(b). An increasing loading rate leads to a higher matrix crack spacing (see also Fig. 4). For instance, the average matrix crack spacing was 0.18 mm for a loading rate of 500 MPa/s, almost twice as large as the average matrix crack spacing at 0.01 MPa/s (0.10 mm). The latter value lies within the values of saturated matrix crack spacing measured for the same composite system by Spearing *et al.*[5] and Sørensen and Holmes,[6] for sustained tensile loading of the order of 10^5 s. Also shown in Fig. 3(b) is the measured average fiber pullout length as a function of loading rate. Contrasting the matrix crack spacing, the fiber pullout length *decreases* with increasing loading rate (see Fig. 5). Note also from Fig. 5 that more debris appears at the fibers and the fracture surfaces at high loading rates. Going back to Fig. 2, the failure strength and strain are also strongly affected by the loading rate. A high loading rate results in a higher failure strength and strain. Finally, from Fig. 2, it can be seen that the toughness (the area under the stress–strain curve) increases with increasing loading rate.

IV. Analysis of Results

In this section we utilize results from simple analytical models to obtain insight into the effect of loading rate on intrinsic microstructural parameters, such as interfacial shear stress and fiber strength. This information will then be used to understand the observed stress–strain behavior of the composite. The models are based on the assumptions of a constant interfacial shear stress and fiber/matrix debonding is neglected.

(1) Stage I: Linear Elastic Behavior

Using the rule of mixtures, the fiber volume fraction, v_f, can be calculated from the initial composite modulus:

$$E_c = v_f E_f + (1 - v_f) E_m \quad (1)$$

where E_c, E_f, and E_m denote the moduli of the undamaged composite, the fibers, and matrix, respectively. From the stress–strain curve (Fig. 2) E_c is found to be 120–129 GPa. Using E_f = 200 GPa and E_m = 98 GPa[14] gives v_f = 22% to 30%. Similar values were calculated from ESEM micrographs taken of the fracture surface, using the areal fraction method. In the following calculations, therefore, we will use v_f = 25%.

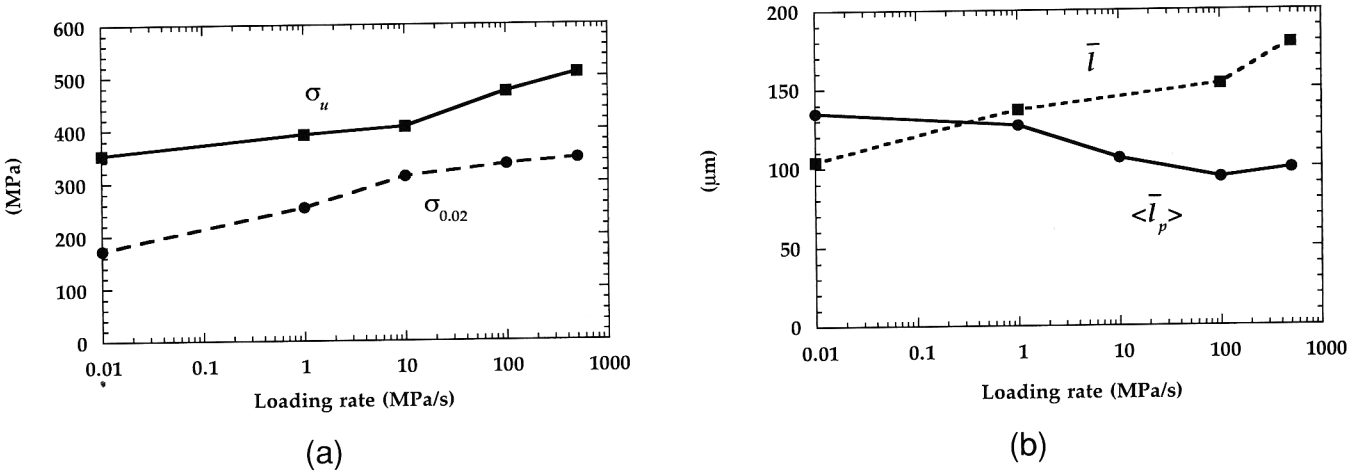

Fig. 3. (a) Measured proportionality stress $\sigma_{0.02}$ and composite strength σ_u as a function of loading rate. Both the proportionality stress and composite strength increase with increasing loading rate. (b) Measured average matrix crack spacing $\bar{l}$ and average fiber pullout length $\langle \bar{l}_p \rangle$ as a function of loading rate. With an increasing loading rate the matrix crack spacing clearly increases, while the pullout length decreases.

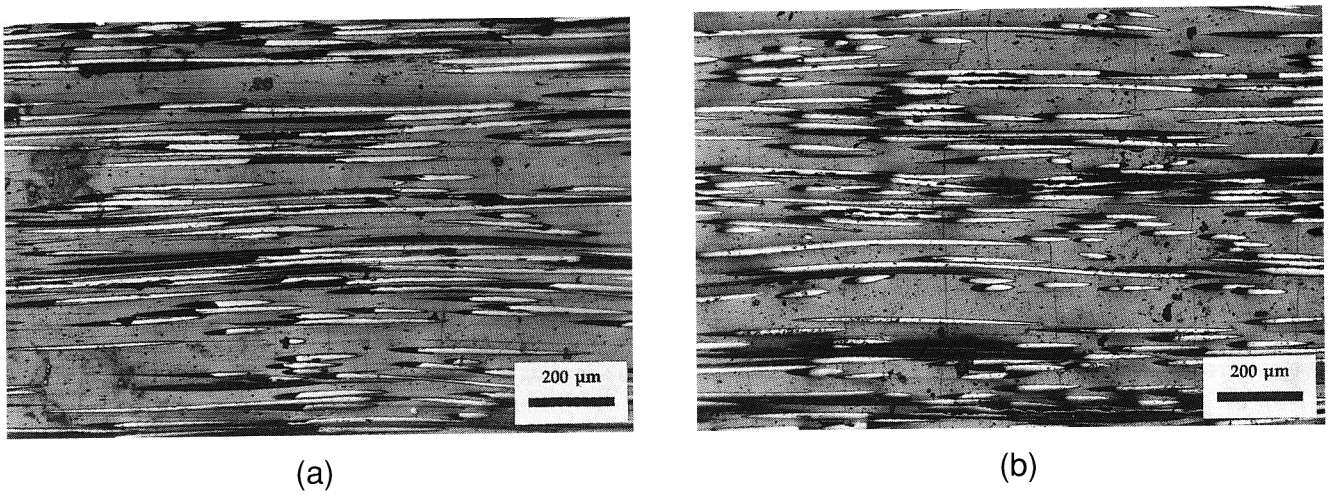

Fig. 4. Micrographs showing the matrix crack spacing for different loading rates: (a) 0.01 MPa/s and (b) 500 MPa/s. Note that a faster loading rate gives a larger matrix crack spacing.

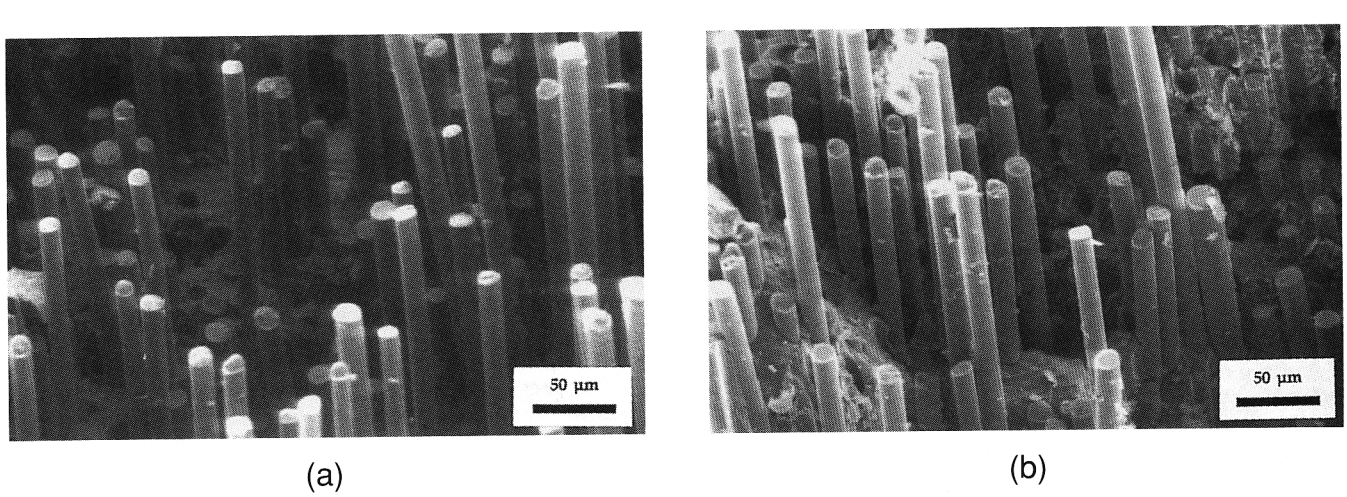

Fig. 5. Micrographs of the specimens fracture surfaces (tilt angle 45°): (a) 0.01 MPa/s, (b) 500 MPa/s. Note that the fiber pullout length decreases with increasing loading rate, and that more debris appears along the fibers at the high loading rate.

(2) Stage II: Nonlinear Behavior

The nonlinearity of the stress–strain curve is attributed to multiple matrix cracking. Matrix cracking in SiC_f/CAS II is known to be time-dependent due to stress corrosion.[5] At a high loading rate, less time is available for matrix cracks to propagate. This appears to be the reason for the increase in matrix crack spacing with increasing loading rate. Note also, from Fig. 1, that Stage II appears to end (when the stress–strain curve regains linearity) at approximately 0.4% strain for a loading rate of 0.01 MPa, increasing to approximately 0.65% strain at a loading rate of 500 MPa/s.

Time-dependent matrix cracking would also affect $\sigma_{0.02}$, since, at a given axial strain, the matrix crack spacing is highest for the specimen loaded at the fastest loading rates (where stress corrosion would be minimal). However, although $\sigma_{0.02}$ represents a well-defined *measurable* quantity, it does not represent a characteristic matrix crack spacing. The matrix crack spacing at $\sigma_{0.02}$ can be estimated by a simple shear-lag model with a pure frictional interface modeled by a constant interfacial shear stress,[15] τ, giving (Appendix A)

$$\bar{l}_{0.02} = 2500\frac{r}{\tau E_f}\left[\frac{(1-v_f)E_m}{v_f E_c}\sigma_{0.02} - \sigma_f^{res}\right]^2 \quad (2)$$

where $\bar{l}_{0.02}$ is the matrix crack spacing, $\bar{l}$, at an applied stress level of $\sigma_{0.02}$, r is the fiber radius, and σ_f^{res} is the axial residual stress in the fiber. From Eq. (2), it follows that for a fixed matrix crack spacing a composite with a higher value of τ gives a higher value of $\sigma_{0.02}$. Physically, the composite acts stiffer with more load transferred onto the matrix.

Although $\sigma_{0.02}$ does not represent a characteristic crack spacing, $\sigma_{0.02}$ *does* imply a certain state of interfacial sliding, namely, when the slip length l_s has reached a characteristic value, $l_{s,0.02}$ (which depends on the actual matrix crack spacing $\bar{l}_{0.02}$), given by (Appendix A)

$$l_{s,0.02} = \frac{1}{100}\sqrt{\frac{\bar{l}_{0.02} r E_f}{\tau}} \quad (3)$$

Later in this paper, after having made estimates of τ, we will use Eqs. (2) and (3) to calculate values of $\bar{l}$ and l_s at $\sigma_{0.02}$.

(3) Stage III: Saturated Matrix Crack Density and Interfacial Sliding

From Fig. 2 it is noted that within the strain range of 0.6% to 0.7%, all stress–strain curves are nearly linear. In earlier studies where acoustic emission was used to detect matrix cracking and fiber failures, it was found that this linear behavior corresponds to a characteristic damage state;[3] the multiple matrix cracking has saturated and the amount of fiber failures is limited. Thus, at a strain value of 0.65% it is reasonable to assume that (A) the matrix crack spacing for all loading rates is similar to the matrix crack spacing measured *after* the tensile fracture and (B) the composite behavior can be described by a model with intact fibers. Using a simple shear-lag model with constant interfacial shear stress and assuming full slip,[3] the difference between the values of the applied stress at the highest and lowest loading rates is (Appendix A)

$$\sigma^{500} - \sigma^{0.01} = \frac{v_f}{2r}(\bar{l}^{500}\tau^{500} - \bar{l}^{0.01}\tau^{0.01}) \quad (4)$$

where superscripts indicate loading rates (in MPa/s). The advantage of using the stress *difference* is that it does not depend on the residual stress, which is not known with good accuracy. Later, we will use Eq. (4) as a consistency check for τ.

(4) Stage IV and Localization: Strength and Fiber Pullout

In the following we use the measured data for the composite strength and average fiber pullout length to estimate how the intrinsic composite parameters (fiber strength and interfacial shear stress τ) are affected by the loading rate. First, however, we must discuss some problems associated with localized fiber failures. When the maximum load is reached, the occurrence of fiber failures leads to further weakening of the composite, such that the fiber failure process is self-sustaining; the rest of the fibers fail rapidly. The final part of the fracture sequence is thus not in static force equilibrium. However, up to the maximum load the experiment occurs under well-defined conditions. Thus, the composite strength, σ_u, can be used as a means to extract intrinsic data. It is more complicated to relate the average fiber pullout length to intrinsic parameters, since a significant number of fibers fail *after* the maximum load, i.e., during localization. The problem is that the different loading conditions (before and after the maximum load) may result in different pullout lengths for fibers breaking before and after the maximum load, since the fiber strength and τ may be velocity-dependent (frictional coefficient and interfacial wear may depend on sliding velocity). From the fracture surfaces we cannot separate fiber failures that occurred before localization (i.e., at a known loading rate) and fiber failures that occurred during localization (unknown pullout velocity).

Analytically, the fraction of broken fiber at the maximum stress can be estimated to be[16]

$$f_b = \frac{2}{m+2} \quad (5)$$

where m is the Weibull modulus describing the strength variation of the fibers. It is, therefore, tempting to assume that the *measured* average pullout length at the fracture surface, $\langle\bar{l}_p\rangle$, is the result of fibers that have failed during a constant loading rate, and the remaining fibers that have failed during localization (see Fig. 6)

$$\langle\bar{l}_p\rangle = \frac{2}{m+2}\bar{l}_p + \frac{m}{m+2}\bar{l}_p^1 \quad (6)$$

where $\bar{l}_p$ represents the "*true*" pullout length associated with the given loading rate, and $\bar{l}_p^1$ represents the pullout length during localization.

We cannot measure $\bar{l}_p^1$. However, since the localized fracture occurs rapidly during a tensile test conducted under load control, we can assume that $\bar{l}_p^1 \approx \langle\bar{l}_p^{500}\rangle$ (superscript 500 denotes the loading rate in MPa/s). Then, using Eq. (6), the "true" pullout lengths can be calculated. These values are listed in Table I.

We can now proceed to use a simple shear-lag model, based on a constant interfacial shear stress τ and describing the fiber strength by a Weibull distribution[17] (σ_0 and m being the characteristic strength and the Weibull modulus, respectively). In the following it is assumed that a possible change in the fiber strength, due to different interfacial velocity, can be adequately described by different values of σ_0, with m being constant. Thus, for each loading rate we assign a different value of σ_0 and τ. It is then easy to show (Appendix B) that

$$\frac{\sigma_0^{500}}{\sigma_0^{0.01}} = \frac{\sigma_u^{500}}{\sigma_u^{0.01}}\left(\frac{\bar{l}_p^{500}}{\bar{l}_p^{0.01}}\right)^{1/m} \quad (7)$$

and

$$\frac{\tau^{500}}{\tau^{0.01}} = \frac{\sigma_u^{500}}{\sigma_u^{0.01}}\frac{\bar{l}_p^{0.01}}{\bar{l}_p^{500}} \quad (8)$$

where superscripts denote loading rates.

For instance, inserting $\bar{l}_p^{500}$, $\bar{l}_p^{0.01}$, σ_u^{500}, $\sigma_u^{0.01}$, and $m = 3$ (from Ref. 18) into Eqs. (7) and (8), we get $\sigma_0^{500}/\sigma_0^{0.01} = 1.16$ and $\tau^{500}/\tau^{0.01} = 2.73$. The results for all loading rates are shown in Fig. 7. The interpretation is clear: The increasing strength with increasing loading rate is due primarily to an increase in τ, *i.e., the interfacial frictional shear stress is velocity-dependent.* Considering that the highest loading rate is 50 000 times the slowest, this variation of τ is perhaps not an unrealistic finding. In fact Cranmer,[19] who measured the friction coefficient of LAS against itself, found that the friction coefficient increased with increasing sliding velocity and suggested that plastic deformation of viscous flow could occur, resulting in increasing friction.

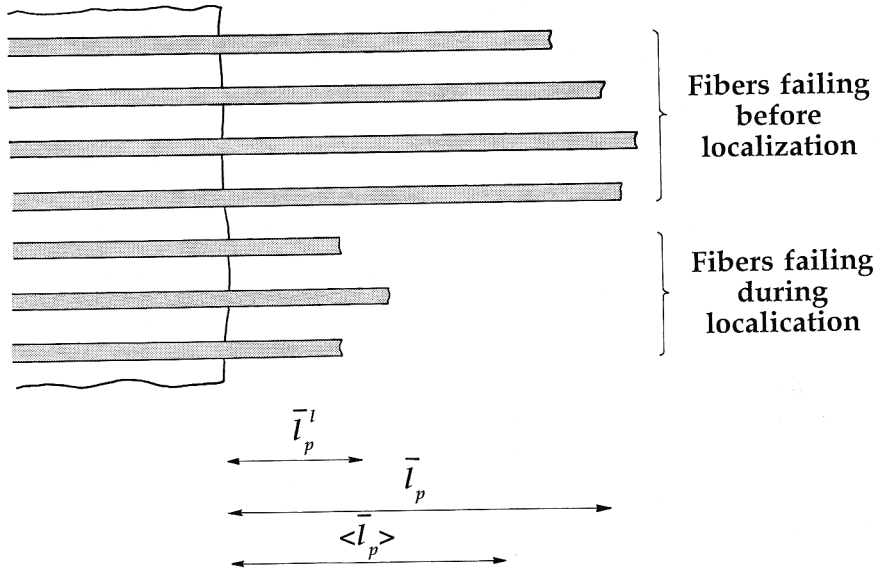

Fig. 6. Measured average fiber pullout length, $\langle \bar{l}_p \rangle$, may be regarded as a weighted sum of the average fiber pullout length that would be present if the fiber failures occurred at a constant loading rate, $\bar{l}_p$ (before localization), and the average fiber pullout length from fibers that fail during localization, $\bar{l}_p^{l}$.

Table I. Measured and Calculated Data from Monotonic Tension Tests as a Function of the Loading Rate

Loading rate (MPa/s)	$\sigma_{0.02}$ (MPa)	$\bar{l}$ (μm)	$\langle \bar{l}_p \rangle$, measured (μm)	$\bar{l}_p$, corrected (μm)
500	345	179	99.4	99.4
100	334	153	93.7	85.2
10	312		106	114
1	253	137	127	168
0.01	173	104	135	189

An increasing interfacial shear stress with increasing loading rate has also been found by single-fiber pullout experiments.[7] The finding that σ_0 remains independent of loading rate suggests that the fibers fail due to preexisting flaws (i.e., not due to wear-induced damage, since that, too, would be expected to be velocity-dependent) and indicates that at room temperature the SiC fibers are not prone to stress corrosion.

The interfacial frictional shear stress τ in Nicalon SiC_f/CAS II has been measured with various techniques to be τ = 10 to 20 MPa for pristine fibers.[20,21] Wang *et al.*[21] reported their single-fiber pushout experiments to be conducted at a loading rate of 300 μN/s, which corresponds to a loading rate of 0.4 MPa/s for a composite with $v_f = 0.25$. This leads us to choose the lowest reported value of τ for $\tau^{0.01}$, viz, $\tau^{0.01} = 10$ MPa, such that we get $\tau^{500} = 27$ MPa.

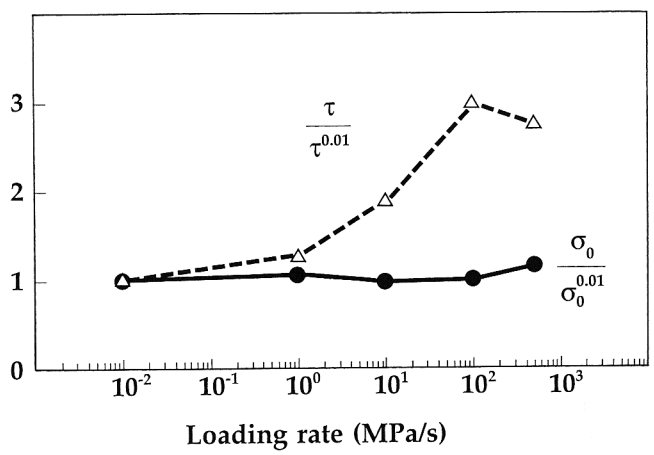

Fig. 7. Calculated values of the intrinsic parameters, τ and σ_0, as functions of the loading rate. The interfacial shear stress τ increases with increasing loading rate, while the fiber strength σ_0 appears to be insensitive to loading rate.

V. Discussion

(1) Proportionality Limit

To give a feel for the damage state at $\sigma_{0.02}$, we can now use the predicted values of τ to calculate the matrix crack spacing and fiber/matrix slip length at $\sigma_{0.02}$. Using Eq. (2) we find that for the highest loading rate (500 MPa/s) $\bar{l}_{0.02}$ is 3.4 mm when the following parameters have been used: $\sigma_{0.02} = 345$ MPa, τ = 27 MPa, $r = 7.5 \times 10^{-6}$ m, $v_f = 0.25$ and $\sigma_f^{res} = -154$ MPa.[22] The lowest loading rate (0.01 MPa/s) corresponds to $\bar{l}_{0.02}$ = 3.0 mm ($\sigma_{0.02} = 173$ MPa). Note, that the values of $\bar{l}_{0.02}$ are quite similar for the two loading conditions, despite a significant difference in stress level. This may be explained by the stress corrosion model.[5] For the slowest loading rate, the loading time (to $\sigma_{0.02}$) is 17×10^3 s and less than 1 s for a loading rate of 500 MPa/s. Thus, with little time available, the effect of stress corrosion is negligible at the high loading rate, but not at the low loading rate. Likewise from Eq. (3), $l_{s,0.02}$ is 0.14 mm and 0.21 mm for loading rates of 500 MPa/s and 0.01 MPa/s, respectively.

(2) Velocity-Dependent Interfacial Shear Stress

Going back to the Stage II behavior, the hypothesis of a velocity-dependent frictional shear stress can be tested. Assuming that the matrix crack spacing at 0.65% strain is identical to that measured from the fracture specimens ($\bar{l}^{500} = 179$ μm and $\bar{l}^{0.01} = 104$ μm) and using the calculated values of τ ($\tau^{0.01} = 10$

MPa and $\tau^{500} = 27$ MPa), predicts a difference in stress levels of 64 MPa. From the experimental stress–strain curves (Fig. 2), the stress difference is found to be 64 MPa. The agreement is outstanding. To prove the point, it can be shown that the measured difference in stress levels at 0.65% strain *cannot* be caused by the difference in matrix crack spacing alone: Assuming $\tau^{500} = \tau^{0.01} = 10$ MPa predicts a stress range of 12.5 MPa, well below the experimental results. All this supports the hypothesis that the interfacial shear stress increases with increasing interface velocity (increasing loading rate). Figure 8 shows the predicted and measured stress differences as functions of the loading rate. The agreement between the predicted and measured values is good.

Despite the fact that Goettler and Faber[7] found τ to increase with increasing loading rate, it has been widely presumed that the interfacial frictional shear stress is independent of velocity.[23] However, the recognition of a velocity-dependent interfacial shear stress has very important implications in practical application of these materials, for instance, in fatigue or impact loading. Under cyclic loading one would expect that a higher loading frequency would lead to an initially higher value of the interfacial shear stress, which might affect the rate of evolution of fatigue damage. Indeed, it has experimentally been found that the fatigue life of continuous-fiber-reinforced ceramics decreases with increasing loading frequency.[24,25] A velocity-dependent frictional shear stress also adds a further complication to how interfacial frictional sliding stresses should be characterized and measured. For impact loading, τ may *decrease* with increasing loading rate if the near-interface matrix is damaged due to the energy dissipation from frictional sliding.[8]

(3) *Additional Comments*

Interfacial *debonding* may also be a time-dependent phenomenon, for instance, due to stress corrosion, such that a higher loading rate could lead to less debonding. This possibility has not been studied in the present work (the models used in this study are based on purely frictional interface response). However, the work by Wang *et al.*[21] on single-fiber pushout experiments on Nicalon SiC_f/CAS II suggests that the interfacial response is adequately described by a pure frictional interface (recall, though, that these experiments were conducted under a rather slow loading rate).

Finally, it should be pointed out that the effect of loading rate on the monotonic stress–strain behavior at elevated temperature may differ significantly from the trends found at room temperature,[26] since at elevated temperatures additional damage mechanisms operate. For example, creep of the fibers and matrix may occur.[27] Moreover, oxidation damage may change the mechanical properties of the fiber/matrix interface, forming strong interface bonding, such that fiber/matrix debonding may no longer occur.[28]

VI. Conclusion

The monotonic stress–strain behavior of a unidirectional SiC_f/CAS II composite was found to be strongly dependent on the applied loading rate. Time-dependent matrix cracking (due to stress corrosion) can explain the decreasing matrix crack spacing with increasing loading rate; it does not explain the increase in composite strength. The increase in composite strength and the decreasing fiber pullout length with increasing loading rate are attributed to an increase in interfacial frictional shear stress with increasing loading rate. Regarding the interfacial shear stress as a velocity-dependent parameter has important implications for understanding the behavior of CMCs, e.g., the evolution of fatigue damage.

APPENDIX A

(1) *Partial Slip*

The longitudinal normal strain for a continuous-fiber-reinforced ceramic matrix composite (Fig. A1) can, under partial slip conditions, be approximated by[15]

$$\varepsilon = \frac{\sigma}{E_c} + \frac{r}{2\bar{l}\tau E_f}\left[\sigma\frac{(1-v_f)E_m}{v_f E_c} - \sigma_f^{res}\right]^2 \tag{A-1}$$

The slip length is[15]

$$l_s = \frac{r}{2\tau}\left[\sigma\frac{(1-v_f)E_m}{v_f E_c} - \sigma_f^{res}\right] \tag{A-2}$$

The definition of $\sigma_{0.02}$ is

$$\varepsilon(\sigma_{0.02}) - \frac{\sigma_{0.02}}{E_c} = 0.02\% \tag{A-3}$$

Combining Eq. (A-1) to (A-3) gives Eqs. (2) and (3).

(2) *Full Slip*

The condition for full slip to occur along the entire interface during a monotonic tension test (Fig. A2) is[15]

$$\sigma \geq \frac{v_f}{1-v_f}\frac{E_c}{E_m}\left[\frac{\bar{l}}{r}\tau + \sigma_f^{res}\right] \tag{A-4}$$

When the composite experiences full slip, the stress–strain relationship is[3,15] (intact fibers)

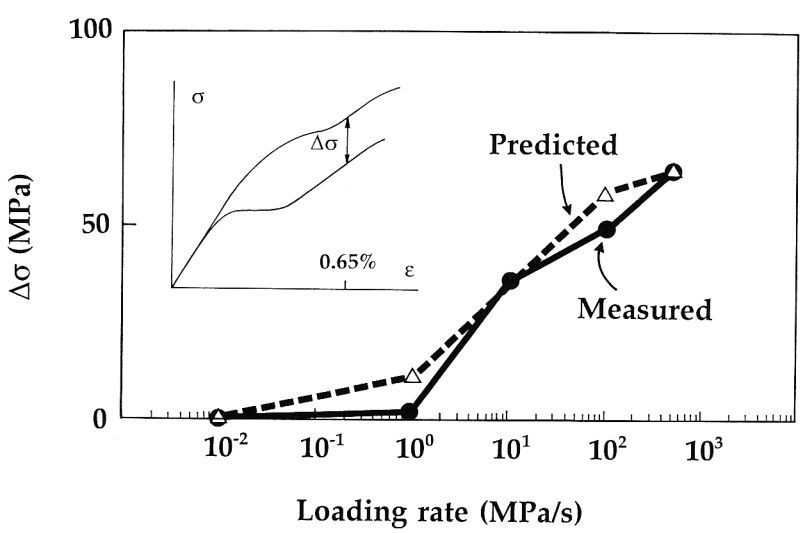

Fig. 8. Measured and predicted values of the stress difference $\Delta\sigma$ at 0.65% strain as a function of loading rate.

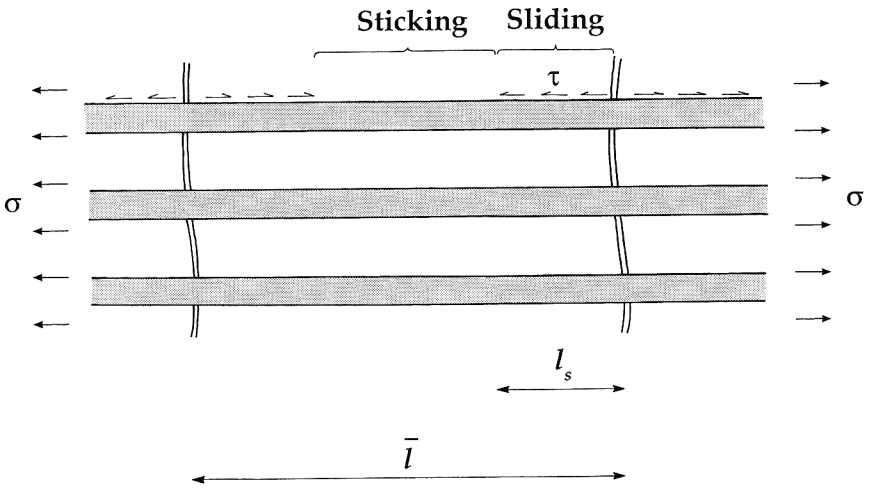

Fig. A1. Model of a continuous-fiber-reinforced ceramic matrix composite with multiple matrix cracking and a constant interfacial shear stress: *partial slip* along the fiber/matrix interface.

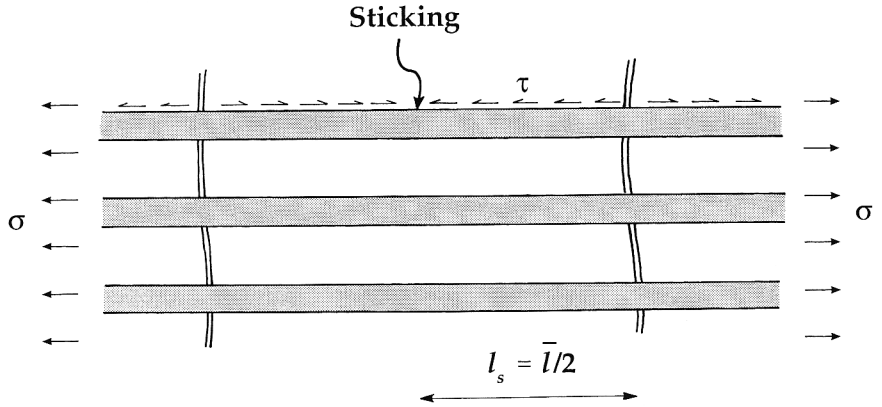

Fig. A2. Model of composite behavior under loading conditions where *full slip* exists along the fiber/matrix interface.

$$\varepsilon = \frac{\sigma}{v_f E_f} - \frac{\bar{l}}{2r}\frac{\tau}{E_f} - \frac{\sigma_f^{res}}{E_f} \tag{A-5}$$

Consider two test specimens at the same strain value, but having different (but fixed) values of τ and $\bar{l}$ and, consequently, different values of σ. Inserting the values into Eq. (A-5) for the two cases and subtracting the two resulting equations gives Eq. (4).

APPENDIX B

According to the model by Thouless and Evans,[17] which is based upon a simple axisymmetric shear-lag model with a constant interfacial frictional shear stress τ, the composite failure strength is proportional to

$$\sigma_u \propto v_f \left(\frac{\sigma_0^m L_0 \tau}{r}\right)^{1/(m+1)} \exp\left(\frac{-1}{m+1}\right) \tag{B-1}$$

where σ_0 and m are the Weibull parameters (the characteristic strength and Weibull modulus, respectively) describing the fracture strength distribution of the fibers for a given gauge length L_0. This model predicts that the average fiber pullout length $\bar{l}_p$ is related to the fiber strength and interfacial sliding shear stress in the following form:

$$\bar{l}_p \propto \left(\frac{\sigma_0 r L_0^{1/m}}{(m+1)\tau}\right)^{m/(m+1)} \Gamma\left(\frac{m+2}{m+1}\right) \tag{B-2}$$

where Γ is the gamma function. We now proceed to use these equations to investigate if the observed difference in composite strength and fiber pullout can be attributed to differences in fiber strength and interfacial shear stress. For simplicity we assume that a possible decrease in composite strength can be adequately described by different values of σ_0, with m being constant. Then the ratio between the strength of the specimen tested under the fastest and slowest loading rates is

$$\frac{\sigma_u^{500}}{\sigma_u^{0.01}} = \left\{\left(\frac{\sigma_0^{500}}{\sigma_0^{0.01}}\right)^m \frac{\tau^{500}}{\tau^{0.01}}\right\}^{1/(m+1)} \tag{B-3}$$

where superscripts denote loading rates.

Likewise, the ratio between the average pullout length of the specimens tested under the highest and lowest loading rates is

$$\frac{\bar{l}_p^{500}}{\bar{l}_p^{0.01}} = \left(\frac{\sigma_0^{500}}{\sigma_0^{0.01}}\frac{\tau^{0.01}}{\tau^{500}}\right)^{m/(m+1)} \tag{B-4}$$

Combining these two equations gives Eqs. (7) and (8).

References

[1]T. A. Michaelske, B. C. Bunker, and S. W. Freiman, "Stress Corrosion of Ionic and Mixed Ionic/Covalent Solids," *J. Am. Ceram. Soc.*, **69**, 217–14 (1986).
[2]J. W. Holmes and C. Cho, "Experimental Observations of Frictional Heating in a Fiber Reinforced Ceramic," *J. Am. Ceram. Soc.*, **75**, 929–38 (1992).
[3]B. F. Sørensen and R. Talreja, "Analysis of Damage in a Ceramic Matrix Composite," *Int. J. Damage Mech.*, **2**, 246–72 (1993).
[4]P. G. Karandikar and T.-W. Chou, "Damage Development and Moduli Reductions in Nicalon–CAS Composites under Static Fatigue and Cyclic Fatigue," *J. Am. Ceram. Soc.*, **73**, 1720–28 (1993).
[5]S. M. Spearing, F. M. Zok, and A. G. Evans, "Stress Corrosion Cracking in a Unidirectional Ceramic-Matrix Composite," *J. Am. Ceram. Soc.*, **77**, 562–70 (1994).
[6]B. F. Sørensen and J. W. Holmes, "Improvement in the Fatigue Life of Fiber-Reinforced Ceramics by Use of Interface Lubrication," *Scr. Metall. Mater.*, **32**, 1393–98 (1995).

[7]R. W. Goettler and K. T. Faber, "Interfacial Shear Stress in Fiber-Reinforced Composites," *Compos. Sci. Technol.*, **37**, 129–47 (1989).

[8]J. Lankford, H. Couque, and A. Nicholls, "Effect of Dynamic Loading on Tensile Strength and Failure Mechanisms in a SiC Fibre Reinforced Ceramic Matrix Composites," *J. Mater. Sci.*, **27**, 930–36 (1992).

[9]S. C. Lim and M. F. Ashby, "Wear-Mechanisms Maps," *Acta Metall.*, **55**, 1–24 (1987).

[10]J. W. Holmes, "A Technique for Tensile Fatigue and Creep Testing of Fiber-Reinforced Ceramics," *J. Compos. Mater.*, **26**, 915–32 (1992).

[11]K. M. Prewo, "Fatigue and Stress Rupture of Silicon Carbide Fiber-Reinforced Glass-Ceramics," *J. Mater. Sci.*, **22**, 2695–701 (1987).

[12]R. Y. Kim and N. J. Pagano, "Crack Initiation in Unidirectional Brittle-Matrix Composites," *J. Am. Ceram. Soc.*, **74**, 1082–90 (1991).

[13]Y. Weitsman and H. Zhu, "Multi-Fracture of Ceramic Composites," *J. Mech. Phys. Solids*, **41**, 351–88 (1993).

[14]I. M. Daniel, G. Anastassopoulos, and J.-W. Lee, "Experimental Micro-Mechanics of Brittle-Matrix Composites"; pp. 133–46 in *Micromechanics: Experimental Techniques*, AMD Vol. 102. Edited by W. N. Sharpe Jr. American Society of Mechanical Engineers, New York, 1990.

[15]A. W. Pryce and P. A. Smith, "Matrix Cracking in Unidirectional Ceramic Matrix Composites under Quasi-Static and Cyclic Loading," *Acta Metall. Mater.*, **41**, 1269–81 (1993).

[16]D. Rouby and P. Reynaud, "Fatigue Behavior Related to the Interface Modification during Load Cycling in Ceramic-Matrix Composites," *Compos. Sci. Technol.*, **48**, 109–18 (1993).

[17]M. D. Thouless and A. G. Evans, "Effects of Pull-Out on the Mechanical Properties of Ceramic-Matrix Composites," *Acta Metall.*, **36**, 517–22 (1988).

[18]K. M. Prewo, "Tension and Flexural Strength of Silicon Carbide Fibre-Reinforced Glass Ceramics," *J. Mater. Sci.*, **21**, 3590–600 (1986).

[19]D. C. Cranmer, "Tribological Properties of Glass-Ceramics," *J. Am. Ceram. Soc.*, **67**, C-180–C-182 (1984).

[20]S.-W. Wang and A. Parvizi-Majidi, "Mechanical Behavior of Nicalon Fiber Reinforced Calcium Aluminosilicate Matrix Composites," *Ceram. Eng. Sci. Proc.*, **11**, 1607–16 (1990).

[21]S.-W. Wang, A. Khan, R. Sands, and A. K. Vasudevan, "A Novel Nano-indenter Technique for Measuring Fiber/Matrix Interfacial Strength in Composites," *J. Mater. Sci. Lett.*, **11**, 739–41 (1992).

[22]B. F. Sørensen and R. Talreja, "Effects of Nonuniformity of Fiber Distribution on Thermally-Induced Residual Stresses and Cracking in Ceramic Matrix Composites," *Mech. Mater.*, **16**, 351–63 (1993).

[23]A. G. Evans and F. W. Zok, "Review: The Physics and Mechanics of Fibre-Reinforced Brittle Matrix Composites," *J. Mater. Sci.*, **29**, 3857–96 (1994).

[24]S. F. Shuler, J. W. Holmes, X. Wu, and D. Roach, "Influence of Loading Frequency on the Room-Temperature Fatigue of a Carbon-Fiber/SiC-Matrix Composite," *J. Am. Ceram. Soc.*, **76**, 2327–36 (1993).

[25]J. W. Holmes, X. Wu, and B. F. Sørensen, "Frequency Dependence of Fatigue Life and Internal Heating of a Fiber-Reinforced Ceramic Matrix Composite," *J. Am. Ceram. Soc.*, **77**, 3284–86 (1994).

[26]S. F. Shuler and J. W. Holmes, "Influence of Loading Rate on the Monotonic Tensile Behavior Fiber-Reinforced Ceramics," Research Memorandum No. 102, September 1990. Ceramic Composites Research Laboratory, Dept. of Mechanical Engineering and Applied Mechanics, 1065 GCBL, The University of Michigan, Ann Arbor, MI 48109–2125.

[27]X. Wu and J. W. Holmes, "Tensile Creep and Creep-Strain Recovery Behavior of Silicon Carbide Fiber/Calcium Aluminosilicate Matrix Ceramic Composites," *J. Am. Ceram. Soc.*, **76**, 2695–700 (1993).

[28]E. Bischoff, M. Rühle, O. Sbaizero, and A. G. Evans, "Microstructural Studies of the Interface Zone of a SiC-Fiber-Reinforced Lithium Aluminum Silicate Glass-Ceramic," *J. Am. Ceram. Soc.*, **72**, 741–45 (1989). □